Apparent secondary-electron emission coefficient and the voltage-current characteristics of argon glow discharges

Z. Donkó

Research Institute for Solid State Physics and Optics, Hungarian Academy of Sciences, P.O. Box 49, H-1525 Budapest, Hungary

The accuracy of secondary-electron emission coefficients, that are used as input data of discharge models, seriously influences the calculated discharge characteristics. As it is very difficult to consider all possible electron emission processes of a cold cathode separately, in most of the recent models an apparent secondary coefficient γ is applied, which is often assumed to be constant, even for a wide range of discharge conditions. In contrast with this common assumption, the present calculations—based on a heavy-particle hybrid model—show that in abnormal glow discharges γ varies considerably with changing discharge conditions: a factor of 3 change of γ has been found in the range of reduced current densities (0.04 mA cm^{-2} Torr$^{-2} \leq j/p^2 \leq 4$ mA cm^{-2} Torr^{-2}) covered in this study. The present simulations also confirm that ionization by heavy particles plays a significant role in the ion production at the abnormal cathode fall. Moreover, it is shown, that the fast heavy particles reflected from the cathode surface play the dominant role in the gas heating.

PACS number(s): 52.80.Hc, 52.65.−y

I. INTRODUCTION

In the last decade a better understanding of the operation of low-pressure dc glow discharges was achieved by the development of complex numerical models. Using fluid and ''electron-ion'' hybrid models—that combine fluid description of slow electrons and ions with particle simulation of fast electrons—several discharge characteristics (e.g., voltage-current curves, electric field distribution, charged particle densities) were calculated in a self-consistent way for various discharge configurations [1–6]. Additional information about cathode sputtering, gas heating, and heavy-particle excitation of spectral lines was also obtained with ''heavy-particle'' hybrid models that include the simulation of the motion and the collisions of heavy particles (typically ions and fast neutrals) [7–13].

The basic input data set of hybrid models consists of collision cross sections, mobility and diffusion coefficients, as well as the operating conditions of the discharge (electrode geometry, pressure, voltage). To calculate the voltage-current density ($V-j$) characteristics of the discharges it is also necessary to prescribe the ratio of the electron (j^-) to ion (j^+) current density at the cathode surface, i.e., an *apparent* secondary-electron emission coefficient:

$$\gamma = \frac{j^-}{j^+}\bigg|_{\text{cathode}}. \tag{1}$$

The several possible electron emission mechanisms (due to the impact of ions, fast atoms, metastable atoms, and ultraviolet photons) are usually not treated separately in most discharge models. Thus the apparent γ has to include the effect of all the relevant mechanisms as accurately as possible, since the calculated discharge characteristics sensitively depend on the value of γ, see, e.g. [14]. As an alternative technique, when the electrical characteristics are known from an experiment, γ can be adjusted to reach agreement between the calculated V-j curves of the discharge and the experimental data [15]. While discharge models have been getting more and more complex in the last years, some of the studies pay marginal attention to the issues related to the secondary-electron emission coefficient(s). In some of the recent papers reporting on sophisticated modeling studies the used value of γ is not even communicated.

For the case of homogeneous electric field ''effective'' electron yield values including the effect of all surface and gas-phase charge-creating processes became recently available [16–19]. However, while these effective yield data (given as a function of reduced electric field E/n) characterize well discharges with uniform electric field, they are not directly applicable for the simulation of discharges with well-developed cathode fall [20].

The primary aim of this paper is to present self-consistent calculations of the apparent γ for cathode-fall conditions in abnormal argon glow discharges, with ''practical'' copper cathode surfaces. The apparent γ for the cathode-fall region is analogous to the effective yield data for homogeneous field. The present calculations of γ are based on a heavy-particle hybrid model, which makes it possible to determine the flux-energy distributions of heavy particles in the cathode sheath. From these distributions γ can readily be obtained using published values of the energy-dependent electron yield of Ar$^+$ ions and fast Ar atoms [16]. For the range of discharge conditions covered in this study, secondary-electron emission due to these two types of particles is dominant. The effect of argon metastables is expected to be at least an order of magnitude less important [16]. Besides the self-consistent calculation of γ, the dependence of the calculated V-j characteristics of the discharge on different modeling assumptions (constant/variable γ, effect of gas-phase heavy-particle processes, and gas heating) is also examined. Section II describes the modeling network, its assumptions and input data, as well as the interfacing of the submodels. The results are presented and discussed in Sec. III, while Sec. IV summarizes the work.

II. DISCHARGE MODEL

The one-dimensional heavy-particle hybrid model consists of (i) a two-component fluid code for Ar^+ ions and slow electrons, (ii) Monte Carlo simulation modules for fast electrons (in order to obtain an accurate ionization source function), argon ions Ar^+ and fast neutral atoms Ar^f (in order to obtain the fluxes and energy distributions of these species at the cathode surface), and (iii) an additional module for the calculation of the gas temperature distribution in the discharge gap.

Molecular ion formation and recombination processes, as well as the backscattering of electrons from the anode are neglected in the model. The electrodes are assumed to be parallel, infinite planes, separated by a distance L. Cathode sputtering is not taken into account due to the relatively low values of the reduced current density.

The principal variables of the fluid model are the positive ion and slow electron densities, $n_i(x)$ and $n_e(x)$, respectively, and the electrostatic potential $V(x)$. These variables can be calculated self-consistently from the continuity and momentum transfer equations for the charged species, and from the Poisson equation (e.g. [3–5])

$$\frac{\partial n_i}{\partial t} + \frac{\partial(n_i \mathbf{v}_i)}{\partial x} = S_i, \tag{2}$$

$$\frac{\partial n_e}{\partial t} + \frac{\partial(n_e \mathbf{v}_e)}{\partial x} = S_e, \tag{3}$$

$$n_i \mathbf{v}_i = n_i \mu_i \mathbf{E} - \frac{\partial(n_i D_i)}{\partial x}, \tag{4}$$

$$n_e \mathbf{v}_e = -n_e \mu_e \mathbf{E} - \frac{\partial(n_e D_e)}{\partial x}, \tag{5}$$

$$\frac{dV}{dx} = -\frac{e}{\epsilon_0}(n_i - n_e), \tag{6}$$

where $\mathbf{v}_e$ and $\mathbf{v}_i$ are the mean velocities, S_e and S_i are the source functions, μ_e and μ_i are the mobilities, and D_e and D_i are the diffusion coefficients of slow electrons and ions, respectively, e is the elementary charge, and ϵ_0 is the permittivity of free space. The mobility of electrons μ_e is taken to be $3 \times 10^5/p$ $cm^2 V^{-1} s^{-1}$ (with p given in Torr) [21], and their diffusion coefficient D_e is chosen to result a fixed 1 eV characteristic energy for slow electrons [3–5]. For the Ar^+ ions, the mobility is taken from [16] and D_i is set to result $D_i/\mu_i = 0.026$ eV $= kT_g$ (at a gas temperature $T_g = 300$ K).

At the solution of the above set of equations the source functions of ions and electrons are needed as input data. In a "pure" fluid approach the source functions are calculated using the "local-field" assumption:

$$S_i(x) = S_e(x) = \alpha_i\left(\frac{E(x)}{n}\right)\phi_e(x), \tag{7}$$

where n is the gas density, α_i is the first Townsend coefficient, and ϕ_e is the electron flux. As the large electric field

gradients near the cathode induce nonequilibrium transport of particles, the ionization source function can be more accurately obtained from Monte Carlo (MC) simulation of the fast electrons [22]. The electrons, that have lost their energy in the negative glow and are no longer able to produce any additional ionization, are transferred from the MC simulation to the slow electron group in the fluid model (see e.g. [3–6]). In order to obtain accurate energy distributions of heavy particles, their motion is traced by Monte Carlo simulation in the cathode sheath, similar to the case of fast electrons.

The elementary processes considered in the Monte Carlo submodels for electrons, positive ions and fast atoms include elastic scattering of the projectiles, as well as excitation and ionization of Ar atoms by the projectiles. The cross sections of the elementary processes—taken from Phelps [23–25]—are reproduced in Fig. 1(a).

The scattering of electrons in elastic momentum transfer and excitation collisions is assumed to be isotropic. In the case of electron impact ionization, the energies of the scattered and ejected electrons, and the directions of their velocity vectors are calculated in accordance with the procedures described in Refs. [26–28].

The cross section of the isotropic part of the elastic Ar^+ + Ar collisions (Q_i) is taken from Ref. [25], while the charge transfer cross section (backward part of elastic scattering, Q_b) is obtained from the momentum transfer cross section (Q_m) as $Q_b = (Q_m - Q_i)/2$ [25]. In isotropic collisions the scattering and azimuth angles are chosen to reflect isotropic scattering in the center-of-mass (c.m.) system. The energy sharing of the collision partners is determined from the scattering angles, see, e.g. [7]. In charge transfer collisions the resulting fast atom keeps the velocity of the incoming ion and the "new" ion is assumed to start from rest.

The cross section of the elastic Ar^f + Ar collision in isotropic approximation is $Q_i^a = (3/2)Q_v$, where Q_v is the viscosity cross section [23]. The calculation of scattering angles and energy sharing is carried out in the same way as in the case of Ar^+ + Ar collisions. The scattering of particles in inelastic heavy-particle collisions is assumed to be isotropic in the c.m. system.

The charge and momentum transfer collisions of heavy particles create fast argon atoms that play a dominant role in the heating of the gas and in the sputtering of the cathode [29]. In the Monte Carlo modules the ions and fast atoms are traced until they reach the cathode surface or—in the case of fast atoms—until their energy falls below a threshold energy (ε_{th}, see later) when they can be considered thermalized. This way the energy of each fast atom and positive ion can be calculated upon arrival to the cathode surface. Besides the ions created in the cathode sheath, the flux of ions arriving from the negative glow is also taken into account.

Let N_i and N_a denote the number of ions and fast atoms arriving to the cathode due to the emission of N_0 primary electrons from the cathode. In stationary state, these ions and fast atoms have to induce the emission of N_0 "new" electrons from the cathode, in order to ensure that the discharge is self-sustained, i.e.,
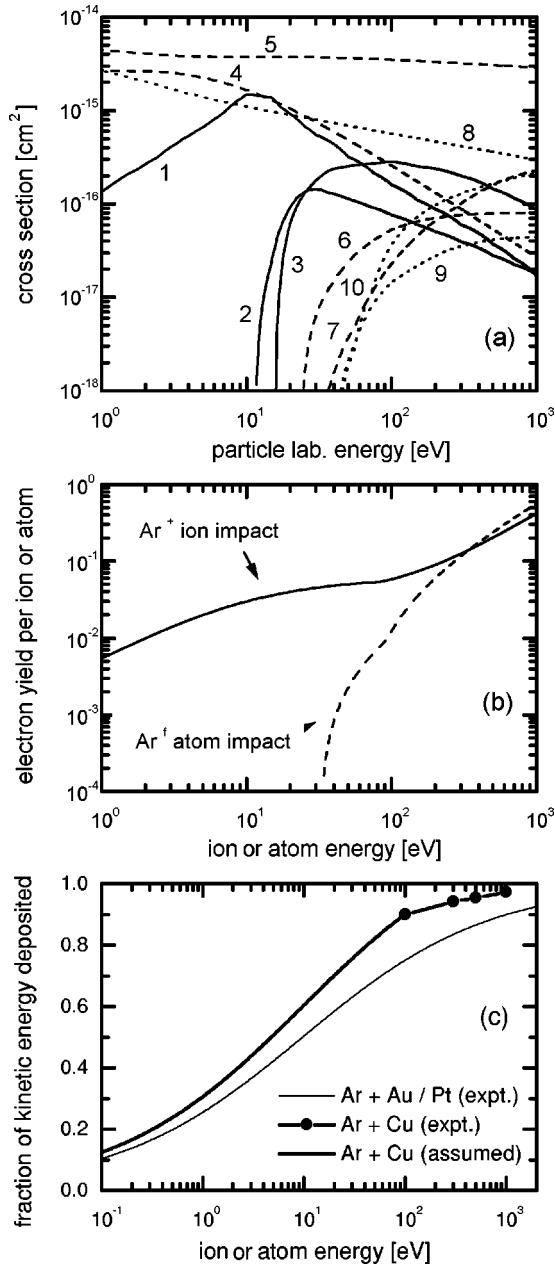
FIG. 1. (a) Cross sections of elementary processes used in the heavy-particle model [23–25]. The solid lines (—) indicate electron collisions (1: elastic, 2: excitation, 3: ionization), the dashed lines (- - -) indicate Ar^+ cross sections (4: isotropic part of elastic scattering, 5: backward elastic scattering, 6: excitation, 7: ionization), and the dotted lines ($\cdots$) indicate fast Ar atom cross sections (8: isotropic elastic scattering, 9: excitation, 10: ionization). (b) Energy dependence of secondary-electron yield due to Ar^+ and Ar^f impact onto "dirty" copper surface [16]. (c) Fractional energy loss of heavy particles bombarding a copper cathode surface. The thin line and the solid circles indicate the experimental data of Refs. [30,31], the heavy line shows the data assumed in the model.

$$\sum_{k=1}^{N_i} \gamma_i(\varepsilon_k) + \sum_{k=1}^{N_a} \gamma_a(\varepsilon_k) = N_0 \qquad (8)$$

must hold, where $\gamma_i(\varepsilon)$ and $\gamma_a(\varepsilon)$ are the energy-dependent

secondary-electron yields (probabilities of the emission of an electron from the cathode due to the impact of a positive ion or a fast atom) and ε_k is the energy of the kth ion or atom. The ratio of the electron to the ion current density at the cathode (being itself the apparent γ) equals to the ratio N_0/N_i, which gives a way to determine γ:

$$\gamma = \frac{\sum_{k=1}^{N_i} \gamma_i(\varepsilon_k) + \sum_{k=1}^{N_a} \gamma_a(\varepsilon_k)}{N_i}. \qquad (9)$$

In the simulations presented here the $\gamma_a(\varepsilon)$ and $\gamma_i(\varepsilon)$ data are taken from Phelps and Petrović [16], and are shown in Fig. 1(b). The data characterize "practical" or "dirty" cathode surfaces. The electron yields of such surfaces can be significantly different compared to those obtained in ion beam experiments with heavily sputtered samples in ultra-high vacuum environment.

After completing the Monte Carlo simulation of fast electrons, ions and fast atoms, the source functions of ions and slow electrons are normalized:

$$S(x) = \frac{j}{e(1+1/\gamma)\Delta x} \frac{N_x}{N_0}, \qquad (10)$$

where j is the current density calculated in the previous fluid cycle, and N_x is the number of ions (slow electrons) created in the slab of width Δx around x due to the emission of N_0 primary electrons from the cathode.

The gas temperature distribution $T_g(x)$ is calculated similarly to the manner described by Revel *et al.* [11]. The heat conductivity equation

$$\frac{d^2 T_g(x)}{dx^2} + \frac{P(x)}{\kappa} = 0, \qquad (11)$$

where $P(x)$ is the gas heating source term and $\kappa = 0.0177$ $W\,m^{-1}\,K^{-1}$, is the thermal conductivity of argon gas, is solved with the following boundary conditions [11]: (1) fixed anode temperature, $T_a = T_g(x=L) = 300$ K, is used and (2) specified temperature gradient in front of the cathode,

$$\kappa \left| \frac{dT}{dx} \right|_{\text{cathode}} = \frac{2\alpha}{2-\alpha} C_p m_p \Delta T_s \frac{n_s v_s}{4} \qquad (12)$$

is assumed, where α is the thermal accommodation coefficient, C_p is the specific heat of the gas at constant pressure, m_p, n_s and v_s are the mass, the density, and the average thermal velocity of Ar atoms in front of the cathode, respectively, and ΔT_s is the "temperature jump" at the cathode surface, i.e., the difference of the cathode temperature T_c and the gas temperature in front of the cathode T_s.

The thermal accommodation coefficient α describes the extent of energy exchange between the cathode and the slow particles colliding with it. At $\alpha=1$ the backscattered particles attain the temperature of the cathode, while at $\alpha=0$ no energy exchange occurs during reflection. For the interaction

of fast particles (that can have energy up to several hundred eV s in the cathode sheath) with the cathode surface different assumptions are used in the modeling literature. In the present model it is assumed that the particles are reflected from the cathode with a fraction of their kinetic energy. The investigations of Winters *et al.* [30] and Coufal *et al.* [31] for different gas (atom and ion) + metal combinations indicate that the fraction of kinetic energy deposited to the cathode increases with the kinetic energy of incoming particles. For argon ions and atoms falling onto a copper surface, only relatively high-energy data ($\varepsilon \geqslant 100$ eV) are available. In the present model the data for Ar + Pt are used for lower energies, scaled up by +20% to fit the higher-energy Ar +Cu data at 100 eV, see Fig. 1(c). Since the fractional energy deposited to the cathode increases with increasing projectile energy, the energy of the reflected particles is rather limited, as it was already pointed out in [32]. Nevertheless, the present study indicates (see later) that the reflected particles (fast atoms and fast neutralized ions) make significant contribution to the heating of the gas, thus their effect cannot be neglected.

The gas heating term $P(x)$—arising from the thermalization of fast heavy particles—is calculated according to the procedures described by Bogaerts *et al.* [12]. The threshold energy, at which a particle is considered to be thermalized, is chosen to be nine times the average thermal energy of argon atoms, $\varepsilon_{th} = 9 \times (3/2) k T_g(x)$.

At the solution of the set of fluid equations (2)–(6) and the heat-conductivity equation the computational grid has a resolution $\Delta x = L/300$. To obtain the self-consistent solution for a given set of discharge conditions the submodels are run iteratively until the stationary state is reached. Most of the results presented in the forthcoming section are obtained with the "full" model. However, some results are also shown, that were obtained neglecting gas-phase heavy-particle processes or gas heating in the calculations. The effect of local-field ionization assumption [Eq. (7)] is also demonstrated.

III. RESULTS

The voltage–reduced-current-density (j/p^2) curves of the argon glow discharge at (pressure)×(electrode separation values) $pL = 0.5$ Torr cm, 1 Torr cm, and 1.5 Torr cm, calculated with the heavy-particle model are plotted in Fig. 2(a). The data are obtained at fixed gas pressure ($p = 1$ Torr) and different electrode separations. In the range of pL values studied the cathode sheath (cathode dark space) and negative glow parts of the discharge exist between the electrodes. The length of the cathode sheath ranges between $d = 0.1$ cm and 0.4 cm, depending on the current density. The rest of the discharge gap is filled by the negative glow. As it can be seen in Fig. 2(a), the discharge voltage depends on pL, a decreasing pL value results in an increasing discharge voltage. At further reduced pL—when the negative glow is getting suppressed—the obstructed discharge mode would be established [33,34]. It can also be seen in Fig. 2(a) that the discharge voltage tends to saturate with increasing j/p^2, especially at higher pL. Above $j/p^2 \approx 4$ mA cm^{-2} Torr^{-2} a
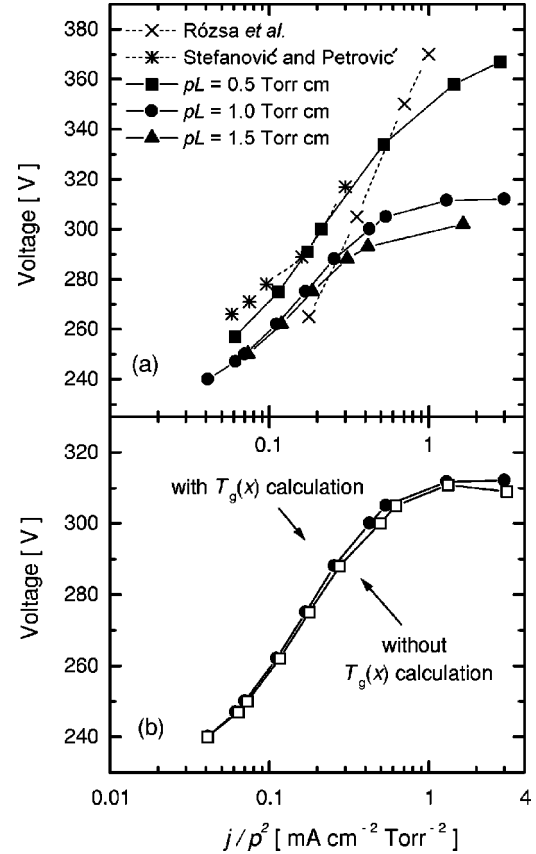
FIG. 2. Voltage–reduced current density characteristics of Ar discharges (a) obtained from the one-dimensional heavy-particle hybrid model for different pL values, and experimental data from the literature: - - $\times$ - - [35] and - - * - - [36]. (b) results of the heavy particle model at $pL = 1$ Torr cm, *with* and *without* gas heating taken into account.

slight negative slope appears for the two highest values of pL. This behavior is caused by the increase of $\gamma_i(\varepsilon)$ and $\gamma_a(\varepsilon)$ with increasing particle energy, see Fig. 1(b). (The energy of particles rises with increasing current density that results in a shortened cathode sheath.)

Two sets of experimental data are also plotted in Fig. 2(a). The voltage-current density data of Rózsa *et al.* [35] were obtained with a 43-mm diameter copper cathode mounted in a six-way metal cross that itself served as the anode. Thus no definite pL value can be assigned to this experiment. In the experiment of Stefanović and Petrović plane-parallel, 54-mm diameter electrodes were used, and the electrical characteristics were measured for different pL values [36]. Their data shown in Fig. 2(a) were obtained at $pL = 0.5$ Torr cm. The results of the present calculations are in very good agreement (within 10 V) with this second set of experimental data, for the range of j/p^2 covered in the experiment. The $V - j/p^2$ curve obtained by Rózsa *et al.* exhibits a steeper slope compared with the results of the present calculations. The slightly lower voltage than the one calculated at $pL = 1-1.5$ Torr cm may be due to the large cathode-anode distance in this experiment. At high currents, on the other hand, the heating of the cathode may be the cause of the increased voltage.
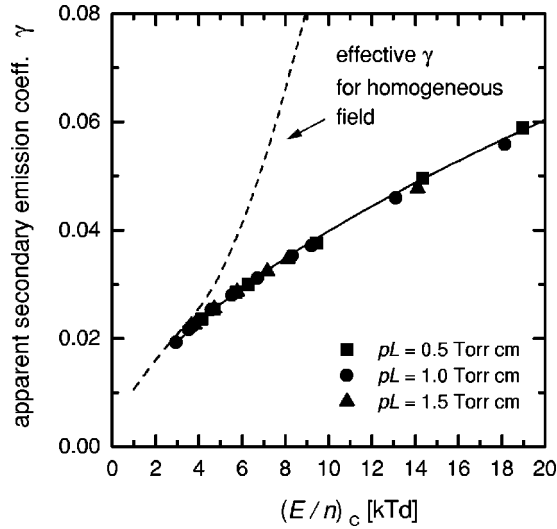
FIG. 3. Apparent secondary-electron emission coefficient as a function of the reduced electric field at the cathode $(E/n)_c$ for different values of pL, and the effective electron yield data of Phelps and Petrović [16] for homogeneous electric field (- - -).

FIG. 4. (a) Comparison of V-j/p^2 curves obtained from the heavy-particle (H-P) and the electron-ion (E-I) hybrid models with different assumptions on γ. The dashed line labeled F shows the characteristics obtained from a "pure" fluid model with $\gamma = 0.06$.

The increased temperature of the cathode surface could easily be included in the model, but because of the lack of experimental data this advantageous feature of the model is not used. Therefore the cathode temperature is assumed to be $T_c = 300$ K throughout the calculations. It has to be mentioned, too, that in the range of currents where gas heating effects and the increased cathode temperature become important, the electrical characteristics of the discharge are expected to depend on the experimental conditions (steady-state or pulsed discharge, cooling of the cathode).

In usual experiments the increasing cathode temperature and/or the radial diffusion loss of charged particles compensates for the saturation/negative slope of the calculated V-j/p^2 curves at high current densities. In fact, when the gas temperature is kept at $T_g = 300$ K in the calculations, a slight negative slope is already observed in the $j/p^2 \geqslant 1$ mA cm^{-2} Torr^{-2} range of reduced current density. This is illustrated in Fig. 2(b) where the V-j/p^2 curve is plotted for $pL = 1$ Torr cm, with and without gas heating taken into account. Apart from avoiding the negative slope, the gas heating only slightly affects the electrical characteristics of the discharge.

The results of the calculations show that the apparent secondary coefficient γ calculated from the flux-energy distribution of heavy particles [Eq. (9)] can be well approximated as a function of the reduced electric field at the cathode surface $(E/n)_c$, regardless of the value of pL, see Fig. 3. Considering all values of pL, the data can be approximated in the 3 kTd $\leqslant (E/n)_c \leqslant 20$ kTd range (1 Td$= 10^{-21}$ Vm^2) by:

$$\gamma = 0.01(E/n)_c^{0.6}. \qquad (13)$$

The fact that γ changes by a factor of 3 in the range of $(E/n)_c$ studied (corresponding to 0.04 mA cm^{-2} Torr$^{-2} \leqslant j$
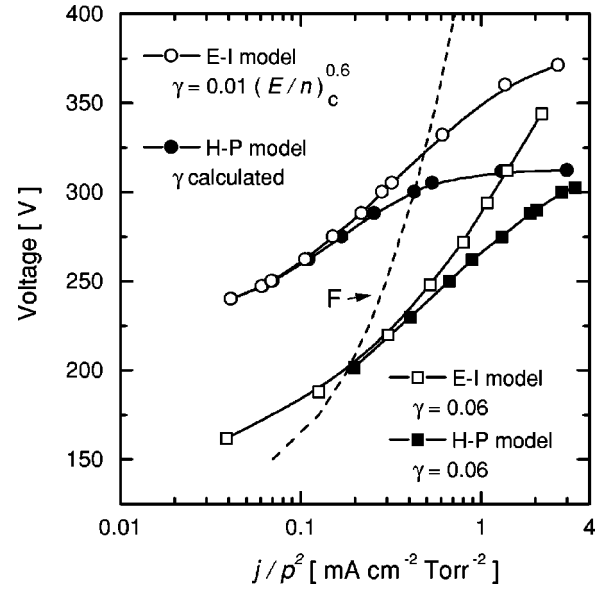
$\leqslant 4$ mA cm^{-2} Torr^{-2}) shows that it would be more appropriate to calculate γ in discharge models rather than using any constant value for it.

The (E/n)-dependent effective electron yield data [16] for homogeneous field are also plotted in Fig. 3. At reduced fields $E/n \approx 3$–4 kTd the apparent γ for the cathode fall is near the effective γ value characterizing a homogeneous field distribution. Under such conditions the cathode fall is relatively long and the gradient of the electric field is relatively small. Consequently the motion of ions and fast atoms is expected to follow the local value of E/n to a reasonable extent. At increased E/n, however, the apparent γ obtained for the cathode fall is well below the effective yield data obtained for homogeneous field, since the energy of heavy particles is lower in the (closely) linearly changing electric field with a peak value of $(E/n)_c$, compared to that in a homogeneous field with $E/n = (E/n)_c$.

Figure 4 compares the V-j/p^2 curves calculated with the heavy-particle hybrid model and an electron-ion hybrid model (that neglects gas-phase heavy-particle processes), for $pL = 1$ Torr cm and taking different assumptions for γ. In the case of the heavy-particle model, besides the calculated γ, the V-j/p^2 curve is also obtained using a fixed value ($\gamma = 0.06$), while the electron-ion model is used with this fixed value of γ and with the apparent yield given by Eq. (13). The heavy-particle model with the constant γ assumption results in about 100 V lower discharge voltage at low currents, compared to the simulation with the calculated γ. A similar difference between the V-j/p^2 curves is found with the electron-ion hybrid model using $\gamma = 0.06$ and taking γ from Eq. (13). The saturation of discharge voltage with increasing j/p^2 is not observed when γ is kept constant (both in the electron-ion hybrid model and in the heavy-particle model). For comparison the V-j/p^2 curve calculated with a "pure"
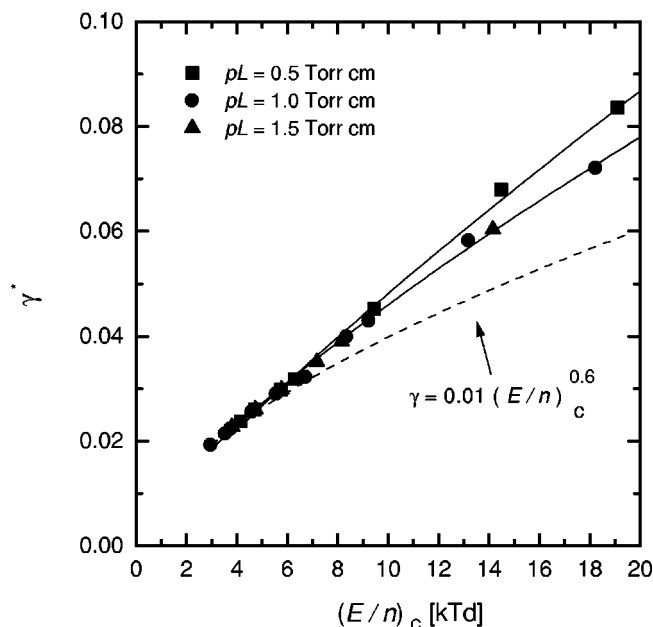
FIG. 5. Values of apparent secondary coefficient γ^* to be used in electron-ion hybrid models to obtain the same V-j/p^2 behavior as predicted by the heavy-particle model with γ calculated in the self-consistent way. The dashed line shows a fit to the results of the heavy-particle model.

fluid model [assuming local-field ionization, Eq. (7)] and using a constant $\gamma = 0.06$ is also plotted in Fig. 4. The results of this model significantly disagree with the results of both the electron-ion and the heavy-particle models.

The difference of the discharge voltage predicted by the electron-ion and heavy-particle models using the same γ is attributed to the effect of heavy-particle ionization: the Ar^+ $+ Ar$ and $Ar^f + Ar$ collisions create additional charges lowering this way the discharge voltage needed to sustain a given current. This effect indicates that the apparent electron yield values obtained from the heavy-particle calculations are not directly applicable in electron-ion hybrid models. To obtain the same V-j/p^2 curves as the ones resulted from the heavy-particle model, an increased emission coefficient γ^* has to be used in electron-ion models. The values of γ^* can be obtained by "turning off" gas-phase heavy-particle processes in the present model, and by adjusting γ to sustain the same current that has been obtained in the simulation including heavy particle processes.

The secondary coefficient γ^*—shown in Fig. 5 as a function of E/n at the cathode surface—is always higher than γ. Unlike in the case of γ, γ^* exhibits a dependence on the value of pL. This dependence is relatively weak until the discharge approaches the obstructed state, when some of the high-energy electrons reach the anode and get absorbed. This is indeed the situation at $pL = 0.5$ Torr cm. In this case the share of heavy-particle ionization becomes more important as it always occurs near the cathode. Taking into account only the γ^* values obtained at $pL = 1$ Torr cm and 1.5 Torr cm, a reasonable approximation for γ^* is given by

$$\gamma^* = 0.008(E/n)_c^{0.76}, \qquad (14)$$
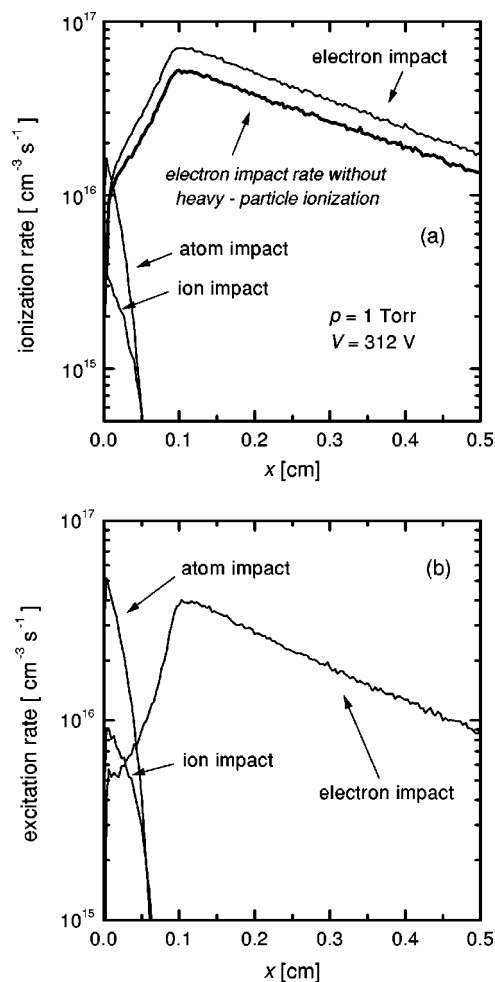
FIG. 6. Contribution of electron/ion/fast atom impact processes to (a) ion production rate and (b) excitation rate. $p = 1$ Torr, $V = 310$ V, $j = 3.1$ mA cm^{-2}. The heavy line in (a) shows a decreased electron impact ionization rate due to neglection of gas-phase heavy-particle processes. (Note that the graphs show only half of the discharge region.)

which is also valid in the 3 kTd$\leq(E/n)_c\leq$20 kTd range. In the case of short gap discharges the use of a somewhat higher γ^* has to be considered.

Figure 6 illustrates the contribution of electron impact and heavy-particle impact processes to the ionization and excitation of the gas. The discharge conditions are $p = 1$ Torr, $L = 1$ cm, $V = 312$ V and $j = 3.1$ mA cm^{-2}. The results indicate that the electron impact ionization/excitation plays the dominant role in the sustainment of ionization and in the creation of light emission from the discharge. Nevertheless, very near the cathode, the major part of excitation is caused by heavy particles, mainly by fast atoms. The overall (spatially integrated) contribution of heavy particles to the total ion production may seem negligible according to the data shown in Fig. 6(a). However, the "extra" electrons created in $Ar^+ + Ar$ and $Ar^f + Ar$ collisions are born very near the cathode and basically behave like primary electrons emitted from the cathode. The ionization caused by these electrons shows up as electron impact ionization rate in Fig. 6. Neglecting these electrons, a significant reduction of the ionization rate
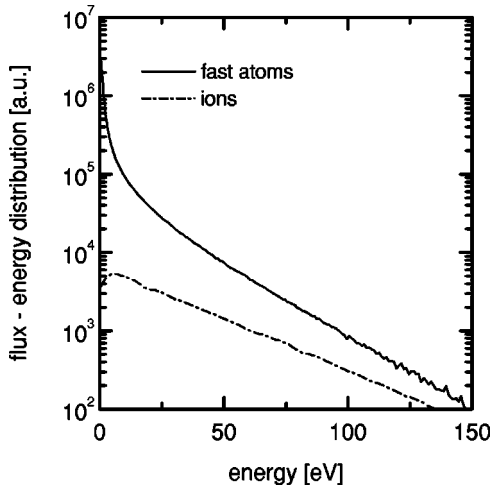
FIG. 7. Flux-energy distribution of heavy particles reaching the cathode surface; $p=1$ Torr, $V=312$ V, $j=1.3$ mA cm^{-2}.

is observed in the simulations, about $\approx 20\%$ for the above set of discharge conditions. Such a difference in the ionization rate explains the deviation of the V-j/p^2 curves calculated from the electron-ion and heavy-particle models.

The flux-energy distribution of heavy particles is plotted in Fig. 7, for $p=1$ Torr, $V=312$ V and $j=1.3$ mA/cm^2. The present results—in agreement with earlier studies—show a high flux of fast atoms, compared to the flux of ions. Part of the ions present in the cathode-fall is created in the cathode fall, while a comparable number of ions flows there from the negative glow (from the region situated at the cathode side of the field-reversal plane [37]).

The gas heating effect of the particles reflected from the cathode can be simply estimated by considering the ions flowing to the cathode sheath from the negative glow. These ions can be accelerated up to the energy corresponding to the full cathode-fall voltage. Due to the Ar$^+$ + Ar collisions, however, very few of them arrive to the cathode with this high energy—most of them deposit their energy to fast atoms. Nevertheless (if we neglect ionization by heavy particles) the total energy available to heat the gas by an ion entering the cathode fall region from the negative glow, corresponds to the cathode fall potential. For the discharge conditions $p=1$ Torr, $V=312$ V and $j=1.3$ mA cm^{-2}, this deposited (heating) energy is found to be only 11 eV/ion (averaged over a high number of ions entering the cathode fall), and the rest of the energy is carried by the particles to the cathode (≈ 300 eV). After reflection from the cathode (where most of the energy is absorbed) the particles still have ≈ 20 eV energy altogether. This amount of energy—which is about twice greater than the energy deposited by the ions and fast atoms on their way towards the cathode—is found to be entirely deposited into the gas.

The power input into the unit volume of the gas (heating term) has been calculated with and without considering the reflection of particles; the results are shown in Fig. 8(a), for $p=1$ Torr, $V=312$ V, $j=1.3$ mA cm^{-2} discharge conditions. The gas temperature profile obtained at the same conditions is plotted in Fig. 8(b). It also shows a considerable difference as an effect of reflected heavy particles. The peak
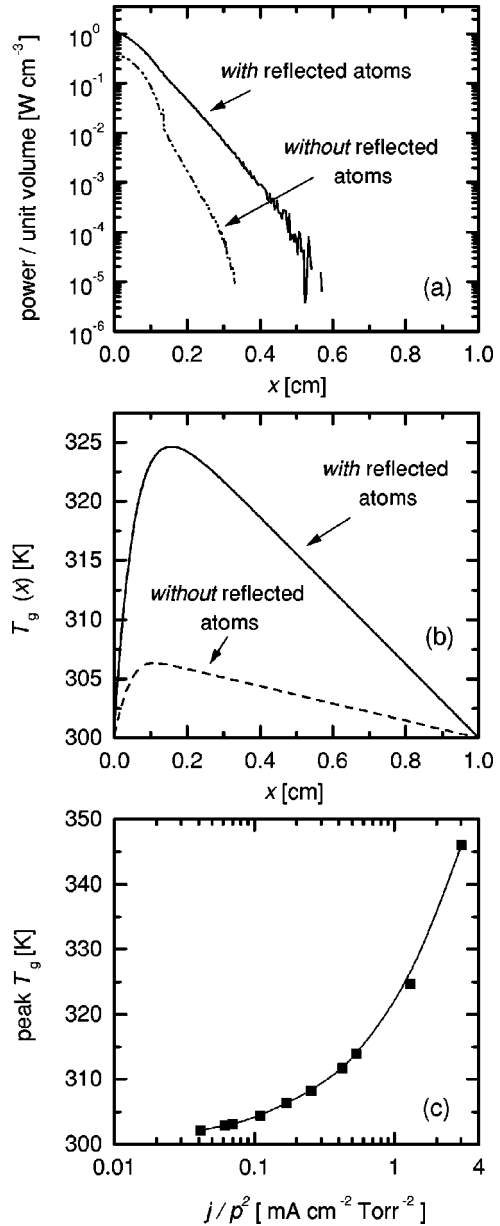
FIG. 8. (a) Power input per unit volume of the gas and (b) gas temperature as a function of distance measured from the cathode *with* (——) and *without* (- - - -) reflected heavy particles taken into account, at $p=1$ Torr, $V=312$ V, $j=1.3$ mA cm^{-2}. (c) Peak value of the gas temperature profile as a function of j/p^2 for $pL=1$ Torr cm.

value of the temperature profile is shown in Fig. 8(c) as a function of reduced current density (with reflected particles taken into account). The results indicate that in the current density range covered in this study the increase of the gas temperature is rather moderate ($\leq 20\%$). It is expected, however, to become important at higher current densities, since T_{peak} increases rapidly with increasing j/p^2. These observations show that the heavy particles reflected from the cathode play a dominant role in the heating of the gas and that an accurate description of the reflection process is essential for accurate gas heating calculations, especially at higher current densities.

IV. SUMMARY

Self-consistent calculations of the apparent secondary co-efficient γ for cathode-fall conditions in an abnormal argon glow discharge are reported. The simulations are based on a hybrid model incorporating gas-phase heavy-particle processes and the calculation of the gas temperature profile. The apparent γ is determined from the flux-energy distribution of Ar^+ ions and fast Ar^f atoms reaching the cathode surface.

It is found that the apparent γ is determined by the reduced electric field at the cathode $(E/n)_c$, and is basically independent of pL. For the range of the reduced current densities covered in this work ($0.04 \ \mathrm{mA \, cm^{-2} \, Torr^{-2}} \leqslant j/p^2 \leqslant 4 \ \mathrm{mA \, cm^{-2} \, Torr^{-2}}$) the apparent γ increases by a factor of 3. This result shows that it is advisable to calculate γ in discharge simulations as carried out in this work—instead of assuming any constant value for it, as done frequently.

The voltage—reduced-current-density $(V\text{-}j/p^2)$ curves for the discharge are obtained for different pL values and with different modeling assumptions. Using the heavy-particle hybrid model it is shown that decreasing pL results in an increasing discharge voltage at given j/p^2. The calculated $V\text{-}j/p^2$ curves show a good agreement with experimental data [35,36]. The comparison of the $V\text{-}j/p^2$ curves obtained with the self-consistently calculated γ and with a constant γ (0.06) show a significant difference of discharge voltage, especially at low currents ($\Delta V \approx 100$ V at $j/p^2 \leqslant 0.1 \ \mathrm{mA \, cm^{-2} \, Torr^{-2}}$). The differences between the electrical characteristics obtained with and without gas-phase heavy-particle processes considered point out the importance of heavy-particle ionization of the gas in the cathode-fall region. It is found that at $j/p^2 \approx 1 \ \mathrm{mA \, cm^{-2} \, Torr^{-2}}$ the integrated ionization rate increases by $\approx 20\%$ due to ionization by heavy particles.

Due to the absence of heavy-particle ionization processes, electron-ion hybrid models predict a higher voltage compared to that calculated with the heavy-particle hybrid model, at the same j/p^2 and using the same γ. This differ-ence can be compensated by using an increased secondary emission coefficient γ^* in electron-ion hybrid models. The values of γ^* are found to exhibit a slight dependence on pL when plotted as a function of $(E/n)_c$.

The calculations show that it is important to take into account the reflection of fast heavy particles from the cathode surface. While the energy of these particles is limited due to the increasing fraction of energy deposited to the cathode, they transfer all their energy to the gas after the reflection. Thus a proper description of the reflection process may be essential for accurate simulations of discharges at higher current densities. The heating of the gas, on the other hand, is found to have relatively small influence on the electrical characteristics of the discharge, for the range of discharge conditions covered in this work.

The apparent secondary emission coefficients obtained here may be used in future electron-ion and heavy-particle models of abnormal glow discharges. It is noted, however, that the accuracy of the present results depends on the uncertainties of the energy-dependent secondary coefficients $\gamma_i(\varepsilon)$ and $\gamma_a(\varepsilon)$ used. These values depend sensitively on the surface conditions of the cathode material. The values used in this work correspond to "practical" or "dirty" cathode surfaces [16]. On the other hand in the case of heated and well annealed surfaces, or different cathode materials (e.g. molybdenium) or different gases (e.g. helium, which has a higher ionization potential and consequently a different behavior of the $\gamma_i(\varepsilon)$ and $\gamma_a(\varepsilon)$ coefficients) the present results may not be directly applicable [38].

[1] J. P. Boeuf, J. Appl. Phys. **63**, 1342 (1988).

[2] M. Surendra, D. B. Graves, and G. M. Jellum, Phys. Rev. A **41**, 1112 (1990).

[3] J. P. Boeuf and L. C. Pitchford, IEEE Trans. Plasma Sci. **19**, 286 (1991).

[4] A. Fiala, L. C. Pitchford, and J. P. Boeuf, Phys. Rev. E **49**, 5607 (1994).

[5] A. Bogaerts, R. Gijbels, and W. J. Goedheer, J. Appl. Phys. **78**, 2233 (1995).

[6] Z. Donkó, Phys. Rev. E **57**, 7126 (1998).

[7] A. Bogaerts, M. van Straaten, and R. Gijbels, Spectrochim. Acta, Part B **50**, 179 (1995).

[8] A. Bogaerts and R. Gijbels, J. Appl. Phys. **78**, 6427 (1995).

[9] A. Bogaerts, R. Gijbels, and W. J. Goedheer, Anal. Chem. **68**, 2296 (1996).

[10] V. V. Serikov and K. Nanbu, J. Appl. Phys. **82**, 5948 (1997).

[11] I. Revel, L. C. Pitchford, and J. P. Boeuf, J. Appl. Phys. **88**, 2234 (2000).

[12] A. Bogaerts, R. Gijbels, and V. V. Serikov, J. Appl. Phys. **87**, 8334 (2000).

[13] Z. Donkó, J. Appl. Phys. **88**, 2226 (2000).

[14] C. Pédoussat, Ph.D. thesis, Paul Sabatier University, Toulouse (1999).

[15] K. Kutasi and Z. Donkó, J. Phys. D **33**, 1081 (2000).

[16] A. V. Phelps and Z. Lj. Petrović, Plasma Sources Sci. Technol. **8**, R21 (1999).

[17] S. Živanov, G. Malović, A. Strinić, and Z. Lj. Petrović, Europhys. Conf. Abstr. **24F**, 134 (2000).

[18] G. Auday, Ph. Guillot, J. Galy, and H. Brunet, J. Appl. Phys. **83**, 5917 (1998).

[19] G. Auday, Ph. Guillot, and J. Galy, J. Appl. Phys. **88**, 4871 (2000).

[20] A. V. Phelps, L. C. Pitchford, C. Pédoussat, and Z. Donkó, Plasma Sources Sci. Technol. **8**, B1 (1999).

[21] A. L. Ward, J. Appl. Phys. **33**, 2789 (1962).

[22] L. C. Pitchford, J. P. Boeuf, P. Segur, and E. Marode, in *Non-*

equilibrium Effects in Ion and Electron Transport, edited by J. W. Gallagher (Plenum, New York, 1990).

[23] A. V. Phelps, ftp://jila.colorado.edu/collision_data

[24] A. V. Phelps, J. Phys. Chem. Ref. Data **20**, 557 (1991).

[25] A. V. Phelps, J. Appl. Phys. **76**, 747 (1994).

[26] S. Yoshida, A. V. Phelps, and L. C. Pitchford, Phys. Rev. A **27**, 2858 (1983).

[27] C. B. Opal, W. K. Peterson, and E. C. Beaty, J. Chem. Phys. **55**, 4100 (1971).

[28] J. P. Boeuf and E. Marode, J. Phys. D **15**, 2169 (1982).

[29] I. Abril, A. Gras-Marti, and J. A. Valles-Abarca, J. Phys. D **17**, 1841 (1984).

[30] H. F. Winters, H. Coufal, C. T. Rettner, and D. S. Bethune, Phys. Rev. B **41**, 6240 (1990).

[31] H. Coufal, H. F. Winters, H. L. Bay, and W. Eckstein, Phys. Rev. B **44**, 4747 (1991).

[32] I. Revel, Ph.D. thesis, Paul Sabatier University, Toulouse, 1999 (unpublished).

[33] Z. Donkó, K. Rózsa, R. C. Tobin, and K. A. Peard, Phys. Rev. E **49**, 3283 (1994).

[34] M. Fukao, M. Ishida, Y. Ohtsuka, and H. Matsuo, Vacuum **59**, 358 (2000).

[35] K. Rózsa, A. Gallagher, and Z. Donkó, Phys. Rev. E **52**, 913 (1995).

[36] I. Stefanović and Z. Lj. Petrović, Jpn. J. Appl. Phys., Part 1. **36**, 4728 (1997).

[37] J. P. Boeuf and L. C. Pitchford, J. Phys. D **28**, 2083 (1995).

[38] A. V. Phelps, Plasma Sources Sci. Technol **10**, 329 (2001).